

## Publisher Correction: Does Predictive coding have a future?





Karl Friston 

Correction to: *Nature Neuroscience* <https://doi.org/10.1038/s41593-018-0200-7>, published online 23 July 2018.

In the version of this article initially published, it was not marked as a Historical News & Views and the supertitle was incorrect. The supertitle should have been “Historical News & Views: Neural Coding.” The error has been corrected in the HTML and PDF versions of the article.

Published online: 22 November 2018  
<https://doi.org/10.1038/s41593-018-0272-4>

## Publisher Correction: Maladaptive cortical hyperactivity upon recovery from experimental autoimmune encephalomyelitis







Erik Ellwardt, Gautam Pramanik, Dirk Luchtman, Tanja Novkovic, Eduardo Rosales Jubal , Johannes Vogt, Isabelle Arnoux , Christina Francisca Vogelaar, Shibajee Mandal, Melanie Schmalz, Zeke Barger, Inigo Ruiz de Azua, Tanja Kuhlmann, Beat Lutz, Thomas Mittmann, Stefan Bittner, Frauke Zipp  and Albrecht Stroh 

Correction to: *Nature Neuroscience* <https://doi.org/10.1038/s41593-018-0193-2>, published online 26 September 2018.

In the version of this article initially published, Inigo Ruiz de Azua's name was miscategorized. His given name is Inigo and his surname is Ruiz de Azua. This has been corrected in the HTML coding.

Published online: 7 November 2018  
<https://doi.org/10.1038/s41593-018-0274-2>

## Publisher Correction: Enhancers active in dopamine neurons are a primary link between genetic variation and neuropsychiatric disease

Xianjun Dong , Zhixiang Liao, David Gritsch, Yavor Hadzhiev , Yunfei Bai, Joseph J. Locascio, Boris Guenewig, Ganqiang Liu, Cornelis Blauwendraat, Tao Wang, Charles H. Adler, John C. Hedreen, Richard L. M. Faull, Matthew P. Frosch, Peter T. Nelson, Patrizia Rizzu, Antony A. Cooper, Peter Heutink , Thomas G. Beach, John S. Mattick , Ferenc Müller  and Clemens R. Scherzer 

Correction to: *Nature Neuroscience* <https://doi.org/10.1038/s41593-018-0223-0>, published online 17 September 2018.

In the version of this article initially published, the legends for Supplementary Figs. 4–8 and 10–14 contained errors. The Supplementary Figure legends have been corrected in the HTML and PDF versions of the article.

### Supplementary Figure 4

Published text: **a**, Distribution and **b**, count of protein-coding mRNAs and non-coding (ncRNAs) expressed in dopamine neurons annotated in GENOCODE v19. **c**, Dopamine neuron transcription factors and the molecular machinery required to produce (dopamine decarboxylase, *DDC*), store (vesicular monoamine transporter 2, *SLC18A1*), and reuptake (dopamine transporter, *SLC6A3*) dopamine from the synaptic cleft was highly expressed in dopamine neurons (bold gene symbols in **d**). **d**, Expression of the twenty most abundant mRNAs and **g**, ncRNAs specific to dopamine neurons (magenta bars) compared to pyramidal neurons (cyan bars) (twenty left-most genes) and vice versa (twenty right-most genes) (note that for each RNA the corresponding bars indicating abundance in the second brain cell type, respectively, are also shown and are close to 0; insert in **d**); median  $\pm$  m.a.d (median absolute deviation) are shown.  $N = 86$  biologically independent dopamine neuron samples and 13 biologically independent pyramidal neuron samples, respectively. See the full list of neuron-specific genes in **Supplementary Table 3**. **e**, The Venn diagram shows the number of mRNAs and **h**, ncRNAs detected exclusively in dopamine neurons (DA), pyramidal neurons (PY), or non-neuronal cells (NN), respectively. **f, i**, The twenty abundant, cell type-exclusive mRNAs (**f**) and ncRNAs (**i**) were sufficient to accurately cluster the 106 individual samples into dopamine, pyramidal, and non-neuronal clusters. DA, substantia nigra dopamine neurons; MCPY, motor cortex pyramidal neurons; TCPY, temporal cortex pyramidal neurons; PBMC, primary human peripheral blood mononuclear cells; FB, primary human fibroblasts.

Corrected: text: **a**, Distribution and **b**, counts of protein-coding mRNAs and non-coding (ncRNAs) expressed in dopamine neurons annotated in GENOCODE v19. **c**, Dopamine neuron transcription factors and the molecular machinery required to produce (dopamine decarboxylase, *DDC*), store (vesicular monoamine transporter 2, *SLC18A1*), and reuptake (dopamine transporter, *SLC6A3*) dopamine

from the synaptic cleft was highly expressed in dopamine neurons (bold gene symbols in **d**). **d**, Expression of the twenty most abundant mRNAs and **g**, ncRNAs specific to dopamine neurons (magenta bars) compared to pyramidal neurons (cyan bars) (twenty left-most genes) and vice versa (twenty right-most genes) (note that for each RNA the corresponding bars indicating abundance in the second brain cell type, respectively, are also shown and are close to 0; insert in **d**); median  $\pm$  m.a.d (median absolute deviation) are shown.  $N = 86$  biologically independent dopamine neuron samples and 13 biologically independent pyramidal neuron samples, respectively. See the full list of neuron-specific genes in **Supplementary Table 4. e**. The Venn diagram shows the number of mRNAs and **h**, ncRNAs detected exclusively in dopamine neurons (DA), pyramidal neurons (PY), or non-neuronal cells (NN), respectively. **f, i**, The twenty abundant, cell type-exclusive mRNAs (**f**) and ncRNAs (**i**) were sufficient to accurately cluster the 106 individual samples into dopamine, pyramidal, and non-neuronal clusters. DA, substantia nigra dopamine neurons; MCPY, motor cortex pyramidal neurons; TCPY, temporal cortex pyramidal neurons; PBMC, primary human peripheral blood mononuclear cells; FB, primary human fibroblasts.

### Supplementary Figure 5

Published text: **a**, Representative dopamine neuron TNEs for which bi-directional CAGE signals were detected in human substantia nigra homogenates. 5,642 dopamine neuron-TNEs had at least 10 detected CAGE reads in both directions in human substantia nigra homogenates in our study;  $N = 4$  biologically independent samples were analyzed. In each panel, the following tracks are displayed: Refseq gene; TNEs calls and normalized RNA-seq density in dopamine neurons (DA); normalized RNA-seq density in pyramidal neurons (PY) and non-neuronal cells (NN); total CAGE counts in substantia nigra homogenates (BRAINcode); combined DNase signal from Roadmap Epigenomics<sup>20</sup>, Integrated Regulation from ENCODE Tracks for H3K27ac, H3K4me1, H3K4me3, and transcription factor ChIP-seq peaks from ENCODE<sup>26</sup>. **b**, Transcription factors with ENCODE ChIP-seq peaks significantly enriched in dopamine neuron TNEs by one-sided Fisher's exact test. ENCODE ChIP-seq peaks were based on the wgEncodeRegTfbsClusteredV3 file downloaded from UCSC Genome Browser, which contains 4,380,444 TF ChIP-seq peaks from 161 TFs in total. The red dash line indicates the significance threshold of Bonferroni-corrected  $P = 0.01$  based on 161 TFs in total. **c-d**, JASPAR binding motifs significantly overrepresented in TNEs. The top 50 canonical transcription factor binding motifs most significantly overrepresented (compared to other transcription factor binding motifs) in all dopamine neuron-TNE (**c**) and in TNE exclusively expressed in dopamine neurons (**d**) are shown (by one-sided Fisher's exact test). Note, bold fonts in (**c**) indicate motifs, whose enrichment was confirmed by a secondary method using randomly selected, length- and GC-matched genomic background sequences for comparison. The y-axis indicates the  $-\log_{10}(P \text{ value})$  from one-sided Fisher's exact test. Red dashed lines indicate the Bonferroni-corrected significance threshold of  $P = 0.01$ . 579 non-redundant vertebrate JASPAR CORE motifs<sup>75</sup> were scanned.

Corrected text: **a**, Representative dopamine neuron TNEs for which bi-directional CAGE signals were detected in human substantia nigra homogenates. 5,642 dopamine neuron-TNEs had at least 10 detected CAGE reads in both directions in human substantia nigra homogenates in our study;  $N = 4$  biologically independent samples were analyzed. In each panel, the following tracks are displayed: Refseq gene; TNEs calls and normalized RNA-seq density in dopamine neurons (DA); normalized RNA-seq density in pyramidal neurons (PY) and non-neuronal cells (NN); total CAGE counts in substantia nigra homogenates (BRAINcode); combined DNase signal from Roadmap Epigenomics<sup>20</sup>, Integrated Regulation from ENCODE Tracks for H3K27ac, H3K4me1, H3K4me3, and transcription factor ChIP-seq peaks from ENCODE<sup>26</sup>. **b**, Transcription factors with ENCODE ChIP-seq peaks significantly enriched in dopamine neuron TNEs by one-sided Fisher's exact test. ENCODE ChIP-seq peaks were based on the wgEncodeRegTfbsClusteredV3 file downloaded from UCSC Genome Browser, which contains 4,380,444 TF ChIP-seq peaks from 161 TFs in total. The red dash line indicates the significance threshold of Bonferroni-corrected  $P = 0.01$  based on 161 TFs in total. **c-d**, JASPAR binding motifs significantly overrepresented in TNEs. The top 50 canonical transcription factor binding motifs most significantly overrepresented (compared to other transcription factor binding motifs) in all dopamine neuron-TNE (**c**) and in TNE exclusively expressed in dopamine neurons (**d**) are shown (by one-sided Fisher's exact test). Note, bold fonts in (**c**) indicate motifs, whose enrichment was confirmed by a secondary method using randomly selected, length- and GC-matched genomic background sequences for comparison. The y-axes indicate the  $-\log_{10}(P \text{ value})$  from one-sided Fisher's exact tests. Red dashed lines indicate the Bonferroni-corrected significance threshold of  $P = 0.01$ . 579 non-redundant vertebrate JASPAR CORE motifs<sup>76</sup> were scanned.

### Supplementary Figure 6

Published text: **a**, Enrichment of VISTA-validated enhancers in TNE overall and the sub-classes of TNEs. Number of enhancer elements is displayed under the bars. Significance in the hypergeometric test is shown above. n.s.: no significant. **b**, Genomic context of a VISTA-confirmed TNE (overlapping with VISTA element hs658) located in intron 3 of the human autism susceptibility candidate 2 gene (*AUST2*). This evolutionary conserved TNE is supported by the classical epigenetic features of a putative active enhancer including open chromatin (DNase)<sup>20</sup>, high levels of H3K4me1 and H3K27ac<sup>26</sup>, low levels of H3K4me3<sup>26</sup>, TF ChIP-seq peak clusters<sup>26</sup>, and sequence conservation. **c**, Genomic context of a TNE located in intron 4 of the Parkinson's gene *SNCA*. It co-localizes with five PD GWAS-derived risk variants. This region is also supported as an active enhancer region by enhancer marks from ENCODE and FANTOM, including high H3K27ac and H3K4me1, open chromatin indicated by DNase I hypersensitivity, hotspot for binding of more than 20 transcription factors, including EP300 (hallmark of active enhancers), RAD21 (a subunit of cohesion complex). GATA transcription factors are known to occupy conserved intronic binding motifs in *SNCA* (Scherzer et al., *PNAS*, 2008). This region is also bi-directionally transcribed as supported by CAGE signal. **d**, UCSC genome browser screenshots of two dopamine neuron-specific TNE, H303 and H305, and two pyramidal neuron-specific TNE, H210 and H211. The exon4-exon5 junction of the *SLC6A3* gene (encoding the dopamine transporter) was evaluated as positive control. For TNEs localized to an intron, the host gene symbol is shown. The displayed tracks are RNA-seq density in dopamine neurons (DA), pyramidal neurons (PY), and non-neuronal cells (NN). The gray box indicates the target transcript region probed by qPCR. Horizontal bars under the RNA-seq density track indicate TNEs calls. The number of spliced reads for the *SLC6A3* e4-e5 junction site is highlighted in the sashimi plot.

Corrected text: **a**, Genomic context of a TNE located in intron 4 of the Parkinson's gene *SNCA*. This TNE co-localizes with five GWAS-derived variants associated with PD risk. It is supported as an active enhancer region by marks from ENCODE and FANTOM, including high H3K27ac and H3K4me1, open chromatin indicated by DNase I hypersensitivity, hotspot for binding of more than 20 transcription factors,

including EP300 (hallmark of active enhancers), RAD21 (a subunit of cohesion complex). GATA transcription factors are known to occupy conserved intronic binding motifs in *SNCA* (Scherzer et al., *PNAS*, 2008). This region is bi-directionally transcribed as supported by CAGE signal. **b**, UCSC genome browser screenshots of two dopamine neuron-specific TNE, H303 and H305, and two pyramidal neuron-specific TNE, H210 and H211. The exon4-exon5 junction of the *SLC6A3* gene (encoding the dopamine transporter) was evaluated as positive control. For TNEs localized to an intron, the host gene symbol is shown. The displayed tracks are RNA-seq density in dopamine neurons (DA), pyramidal neurons (PY), and non-neuronal cells (NN). The gray box indicates the target transcript region probed by qPCR. Horizontal bars under the RNA-seq density track indicate TNEs calls. The number of spliced reads for the *SLC6A3* e4-e5 junction site is highlighted in the sashimi plot. **c**, Enrichment of VISTA-validated enhancers in TNE overall and the sub-classes of TNEs. Number of enhancer elements is displayed under the bars. Significance in the hypergeometric test is shown above. n.s.: no significant. **d**, Genomic context of a VISTA-confirmed TNE (overlapping with VISTA element hs658) located in intron 3 of the human autism susceptibility candidate 2 gene (*AUST2*). This evolutionary conserved TNE is supported by the classical epigenetic features of a putative active enhancer including open chromatin (DNase)20, high levels of H3K4me1 and H3K27ac26, low levels of H3K4me326, TF ChIP-seq peak clusters26, and sequence conservation.

#### Supplementary Figure 7

Published text: **a**, UCSC genome browser screenshot for the *VMP1-MIR21* locus in humans (left) and its two main ortholog loci in zebrafish (right). The human locus has two ortholog copies in zebrafish due to a whole genome duplication event in the teleost fish. These are shown as the two long chained alignments in the dot frames (chr15+16277k and chr10-28843k, respectively). The TNE element we tested in zebrafish (*VMP1-TNE*) is marked in magenta. It is conserved on the zebrafish chr10 ortholog. Zoom-in details for the two zebrafish orthologs are shown on right. Note that the ortholog gene *vmp1* is absent on the chr10 copy (the dot frame in the bottom right panel). **b**, Schematic of evolutionary changes in the *VMP1-MIR21* locus following the whole genome duplication event in teleost fish. The *MIR-21* gene resides adjacent to *VMP1* and is in conserved synteny with the *VMP1-TNE* ortholog in zebrafish, suggesting that this candidate regulatory element may be shared between *VMP1* and *miR-21* or specifically target the *miR-21* promoter. The *VMP1-TNE* element is highlighted in magenta and *miR21* is highlighted in blue.

Corrected text: **a**, UCSC genome browser screenshot for the *VMP1-MIR21* locus in humans (left) and its two main ortholog loci in zebrafish (right). The human locus has two ortholog copies in zebrafish due to a whole genome duplication event in the teleost fish. These are shown as the two long chained alignments in the dot frames (chr15+16277k and chr10-28843k, respectively). The TNE element we tested in zebrafish (*VMP1-TNE*) is marked in magenta. It is conserved on the zebrafish chr10 ortholog. Zoom-in details for the two zebrafish orthologs are shown on right. Note that the ortholog gene *vmp1* is absent on the chr10 copy (the dot frame in the bottom right panel). **b**, Schematic of evolutionary changes in the *VMP1-MIR21* locus following the whole genome duplication event in teleost fish. The *miR-21* gene resides adjacent to *VMP1* and is in conserved synteny with the *VMP1-TNE* ortholog in zebrafish, suggesting that this candidate regulatory element may be shared between *VMP1* and *miR-21* or specifically target the *miR-21* promoter. The *VMP1-TNE* element is highlighted in magenta and *miR21* is highlighted in blue.

#### Supplementary Figure 8

Published text: **a**, GWAS diseases and traits significantly enriched in dopamine TNEs and its subclasses; one-sided Fisher's exact test. **b**, Density of dopamine system traits, seizure disorders, and autoimmune diseases in each of the three cell types. Trait density was calculated as for Fig. 5 based on the significant over-localization of GWAS variants for each of the three disease ontologies in TNE of each cell type. Comparison of cell types revealed that traits of the dopamine system were relatively more enriched in dopamine neuron-TNE compared to TNE expressed in pyramidal neurons and non-neuronal cells (e.g. Parkinson's disease, addiction, response to methylphenidate and iloperidone). Seizure disorders (epilepsy, partial epilepsy, and febrile seizures) and autoimmune diseases, however, showed preferential enrichment in pyramidal neuron-TNE and non-neuronal cell-TNE, respectively.

Corrected text: GWAS diseases and traits significantly enriched in dopamine TNEs and its subclasses; one-sided Fisher's exact test.

#### Supplementary Figure 10

Published text: **a**, Manhattan plot of eQTL SNPs in association with TNEs (top panel), ncRNAs (middle panel), and mRNAs (bottom panel). SNPs with the best eQTL *P*-values in the local genomic regions are shown as diamonds. The color of the diamond indicates if the associated gene is related with nervous system disease (red), other Mendelian disease (blue), or non-Mendelian disease (grey), respectively. Thirteen of the 151 cis-regulated TNEs were expressed from host genes mutated in Mendelian diseases (TNE-eQTLs, *top Manhattan plot*), 10 (69%) of which are nervous system diseases (red diamonds). These TNE host genes included *NRXN1* (MIM 600565) linked to rare autosomal recessive mental retardation and susceptibility to schizophrenia and *CACNB4* (MIM 601949), mutated in autosomal dominant types of episodic ataxia and juvenile myoclonic epilepsy. 3,381 ncRNA-eQTLs were significant, comprising combinations of 3,320 unique eSNPs and 52 unique expressed ncRNA genes (ncRNA-eQTLs, *middle Manhattan plot*). 1,150 mRNA-eQTLs reached statistical significance, comprising combinations of 676 unique eSNPs and 46 unique associated expressed protein-coding genes (mRNA-eQTLs, *bottom Manhattan plot*). *ATP5A1*, *CRYGC*, and *ADAMTS18*, all of which are mutated in Mendelian diseases, exhibited significant mRNA-eQTL associations in dopamine neurons. *P* values from the linear regression model implemented in Matrix-eQTL are shown; FDR 0.05, red dashed line. **b**, TNE-eQTL boxplots visualizing TNE expression values by genotype for eight TNE physically localized to introns of familial neurologic disease genes. *P*-values are from Matrix-eQTL linear regression model; *N* = 84 biologically independent samples. Box plots as in Fig. 3b.

Corrected text: **a**, Manhattan plot of eQTL SNPs in association with TNEs (top panel), ncRNAs (middle panel), and mRNAs (bottom panel). SNPs with the best eQTL *P*-values in the local genomic regions are shown as diamonds. The color of the diamond indicates if the associated gene is related to nervous system disease (red), other Mendelian disease (blue), or non-Mendelian disease (grey), respectively. Thirteen of the 151 cis-regulated TNEs were expressed from host genes mutated in Mendelian diseases (TNE-eQTLs, *top Manhattan plot*), 10 (69%) of which are nervous system diseases (red diamonds). These TNE host genes included *NRXN1* (MIM 600565) linked to rare autosomal recessive mental retardation and susceptibility to schizophrenia and *CACNB4* (MIM 601949), mutated in autosomal

dominant types of episodic ataxia and juvenile myoclonic epilepsy. 3,381 ncRNA-eQTLs were significant, comprising combinations of 3,320 unique eSNPs and 52 unique expressed ncRNA genes (ncRNA-eQTLs, *middle Manhattan plot*). 1,150 mRNA-eQTLs reached statistical significance, comprising combinations of 676 unique eSNPs and 46 unique associated expressed protein-coding genes (mRNA-eQTLs, bottom *Manhattan plot*). *ATP5A1*, *CRYGC*, and *ADAMTS18*, all of which are mutated in Mendelian diseases, exhibited significant mRNA-eQTL associations in dopamine neurons. *P* values from the linear regression model implemented in Matrix-eQTL are shown; FDR 0.05, red dashed line. **b**, TNE-eQTL boxplots visualizing TNE expression values by genotype for eight TNE physically localized to introns of familial neurologic disease genes. *P*-values are from Matrix-eQTL linear regression model; *N* = 84 biologically independent samples. Box plots as in Fig. 3b.

#### Supplementary Figure 11

Published text: Each dot is a SNP-gene pair. Only pairs for genes and SNPs within the *MAPT* locus (chr17:43000000-45300000 in hg19) are displayed. Y-axis is the  $-\log_{10}(p\text{-value})$  of original eQTL analysis (without conditional analysis), and X-axis is the  $-\log_{10}(p\text{-value})$  of conditional eQTL analysis after adjusting the rs17649553 SNP. Horizontal and vertical dash line is for *p*-value cutoff with FDR of 0.05. *P*-values are from the linear regression model implemented in Matrix-eQTL; *N* = 84 biologically independent samples. Majority of significant eSNPs become insignificant after conditional analysis of rs17649553, except 31 SNPs in the *KANSL1* gene (green dots on the top-right corner) rs17698176 in *NSF* (red dot on the top-right corner). The 31 SNPs are in the same LD block as rs17649553. Coordinates of LD block: LD2, chr17:43657257-44369320; LD3, chr17:44762252-44862613.

Corrected text: Each dot represents an SNP-transcript pair. Only pairs of transcripts and SNPs within the *MAPT* locus (chr17:43000000-45300000 in hg19) are displayed. Y-axis is the  $-\log_{10}(p\text{-value})$  of original eQTL analysis (without conditional analysis), and X-axis is the  $-\log_{10}(p\text{-value})$  of conditional eQTL analysis after adjusting the rs17649553 SNP. Horizontal and vertical dash line is for *p*-value cutoff with FDR of 0.05. *P*-values are from the linear regression model implemented in Matrix-eQTL; *N* = 84 biologically independent samples. The majority of significant eSNPs became insignificant after conditional analysis of rs17649553, except 31 SNPs in the *KANSL1* gene (green dots on the top-right corner) and rs17698176 in *NSF* (red dot in the top-right corner). The 31 SNPs are in the same LD block as rs17649553. Coordinates of LD block: LD2, chr17:43657257-44369320; LD3, chr17:44762252-44862613.

#### Supplementary Figure 12

Published text: **a**, This eQTL relation between rs17649553 and *KANSL1-TNE1* and *LRRC37A4P* was confirmed by a second method, qPCR, in laser-captured dopamine neurons. **b**, Moreover, the association was replicated in a second, independent population representing pyramidal neurons laser-captured from temporal cortex of 31 high-quality control brains. The geometric mean of the two standard housekeeping genes, *EIF4A2* and *RPL13*, was used to control for input RNA in (**a**) and (**b**); *P* values by two-tailed Student's *t*-tests. Mean  $\pm$  SEM are shown. **c,d**, Furthermore, the rs17649553-LRRC37A4P eQTL association was confirmed *in silico* in a third independent population comprising 56 substantial nigra (**c**) as well 96 frontal cortex (**d**) samples from the GTEx data set, which used a polyA+ selecting protocol that would not detect *KANSL1-TNE1*. *P* values by two-tailed Student's *t*-tests. Box plots as in Fig. 3b.

Corrected text: **a**, This eQTL relation between rs17649553 and *KANSL1-TNE1* and *LRRC37A4P* was confirmed by a second method, qPCR, in laser-captured dopamine neurons. **b**, Moreover, the association was replicated in a second, independent population representing pyramidal neurons laser-captured from temporal cortex of 31 high-quality control brains. The geometric mean of the two standard housekeeping genes, *EIF4A2* and *RPL13*, was used to control for input RNA in (**a**) and (**b**); *P* values by two-tailed Student's *t*-tests. Mean  $\pm$  SEM are shown. **c,d**, Furthermore, the rs17649553-LRRC37A4P eQTL association was confirmed *in silico* in a third independent population comprising 56 substantial nigra (**c**) as well 96 frontal cortex (**d**) samples from the GTEx data set, which used a polyA+ selecting protocol that would not detect *KANSL1-TNE1*. *P* values by two-tailed Student's *t*-tests. Box plots as in Fig. 3b.

#### Supplementary Figure 13

Published text: **a**, Genotyping pipeline. 93 subjects were initially genotyped on Illumina HumanOmni2.5 Exome BeadChips. After a series of sample and variant quality control steps, 6,124,720 SNPs for each of 91 subjects were retained for downstream eQTL analysis. **b**, Pipeline for eQTL analysis of TNE, ncRNAs, and mRNAs across 86 dopamine neuron samples.

Corrected text: **a**, Genotyping pipeline. 93 subjects were initially genotyped on Illumina HumanOmni2.5 Exome BeadChips. After a series of sample and variant quality control steps, 6,124,720 SNPs for each of 91 subjects were retained for downstream eQTL analysis. **b**, Pipeline for eQTL analysis of TNE, ncRNAs, and mRNAs across 84 dopamine neuron samples.

#### Supplementary Figure 14

Published text: **a**, Dopamine neuron samples (DA) (*N* = 86) were merged using the trimmed mean of RNA-seq density at each nucleotide position. Pyramidal neuron samples (from motor or temporal cortex; *N* = 13) were similarly merged. Non-neuronal cell samples (from white blood cells and fibroblasts; *N* = 7) were similarly merged. Genome-wide scanning using the six-step method identified TNE sets for each group. **b**, Histogram of RNA-seq density (RPM) across 1,000,000 randomly selected single nucleotides. The histogram was fitted into a normal distribution that was used to determine the local summit cutoff with *P* = 0.05 (informing step #2 of the TNE identification method).

Corrected text: **a**, Dopamine neuron samples (DA) (*N* = 86) were merged using the trimmed mean of RNA-seq density at each nucleotide position. Pyramidal neuron samples (from motor or temporal cortex; *N* = 13) were similarly merged. Non-neuronal cell samples (from white blood cells and fibroblasts; *N* = 7) were similarly merged. Genome-wide scanning using the six-step method identified TNE sets for each group. **b**, Histogram of RNA-seq density (RPM) across 1,000,000 randomly selected single nucleotides. The histogram was fitted into a normal distribution that was used to determine the local summit cutoff with *P* = 0.05 (informing step #2 of the TNE identification method).

Published online: 17 December 2018

<https://doi.org/10.1038/s41593-018-0277-z>